



## Research article

# Clay mineral nanostructures regulate sequestration of organic carbon in typical fluvial sediments

Hongzhe Song<sup>a</sup>, Zhifei Liu<sup>a,\*</sup>, Baozhi Lin<sup>a</sup>, Yulong Zhao<sup>a</sup>, Fernando P. Siringan<sup>b</sup>, Chen-Feng You<sup>c</sup>

<sup>a</sup> State Key Laboratory of Marine Geology, Tongji University, Shanghai, 200092, China

<sup>b</sup> Marine Science Institute, University of the Philippines, Diliman, Quezon City, 1101, Philippines

<sup>c</sup> Department of Earth Sciences, National Cheng Kung University, Tainan, 70101, Taiwan

## ARTICLE INFO

## Keywords:

Smectite  
Illite  
Layer structure  
Fluvial sediments  
Taiwan  
Luzon

## ABSTRACT

The association between clay minerals and organic carbon is pivotal for understanding transport, burial, and preservation processes of sedimentary organic carbon. However, fine-scale microscopic studies are still limited in assessing the effect of diverse clay mineral structures and properties on organic carbon sequestration. In this study, we employed X-ray photoelectron spectroscopy, Fourier transform infrared spectroscopy, and transmission electron microscopy coupled with energy dispersive spectroscopy and electron energy loss spectroscopy analyses to investigate the nanoscale interaction between clay minerals and organic carbon of two typical fluvial sediment samples with contrasting clay mineral compositions and organic carbon origins. Sample from Taiwan shows abundant illite and chlorite with petrogenic organic carbon, while sample from Luzon has significant smectite with pedogenic organic carbon. We observed that the nanostructure of the clay minerals controls the distribution of organic carbon. In the Luzon sample, the organic carbon is tightly associated with smectite, occupying expandable interlayer spaces. In the Taiwan sample, however, the organic carbon is primarily confined on the surface and edge of illite. These findings offer valuable insights into the selective association of organic carbon with clay minerals and underscore the role of clay mineral nanolayer structures in governing the occurrence and preservation of organic carbon in sediments. A comprehensive understanding of these interactions is crucial for accurate assessments of carbon cycling and sequestration in the natural environment.

## 1. Introduction

The association between clay minerals and organic carbon plays a significant role in carbon burial, transport, and preservation. Recent studies have shown that 90 % of soil organic matter is closely related to clay minerals, which protect organic matter from decomposition in the soil environment, thereby exerting an important influence on regulating the release of CO<sub>2</sub> from the soil to the atmosphere [1–4]. Further, in the transport of organic carbon from the river to the ocean, physical protection and interfacial chemical reaction prevention of clay mineral aggregates are also important factors for avoiding rapid decomposition [5,6].

The interaction between clay minerals and organic carbon is controlled by their physical and chemical properties [7,8]. Various

\* Corresponding author.

E-mail address: [lzhifei@tongji.edu.cn](mailto:lzhifei@tongji.edu.cn) (Z. Liu).

<https://doi.org/10.1016/j.heliyon.2024.e25825>

Received 20 November 2023; Received in revised form 2 February 2024; Accepted 2 February 2024

Available online 3 February 2024

2405-8440/© 2024 The Authors. Published by Elsevier Ltd. This is an open access article under the CC BY-NC-ND license (<http://creativecommons.org/licenses/by-nc-nd/4.0/>).

structures and properties of clay minerals exhibit the diversity of their affinity with different types of organic carbon [9–12]. Factors such as specific surface area and cation composition of clay minerals, physical and chemical properties of organic carbon, and microbial composition of environment all play important roles in the organic-mineral interactions [13,14]. Among these factors, the specific surface area of minerals is considered to have the most significant impact on the binding of organic carbon. Numerous research data reveal a strong positive correlation between the specific surface area and the binding of organic carbon [15–17]. Clay minerals, with fine particles and platy morphology, have larger specific surface areas compared to other lithogenic minerals. In particular, the smectite group, besides its extensive external surface area, possesses expandable interlayer domains that can provide several times more adsorption spaces for organic carbon under suitable conditions [18,19]. Therefore, smectite is the most efficient agents for the transport and preservation of organic carbon.

Kennedy et al. conducted a correlation analysis between the internal and external surface areas of minerals and the total organic carbon in black shales [20]. Their study revealed that the internal surfaces of clay minerals, which are difficult to detect using conventional gas adsorption methods, may serve as important locations for organic carbon attachment and adsorption. Further investigations confirmed the close association between clay minerals and organic carbon, providing evidence for the existence of clay mineral-organic carbon interlayer complexes [21]. In recent years, TEM has been used to study nanopores between mineral particles in sedimentary rocks and their relationship with the occurrence of organic carbon [22,23]. However, the spatial resolution limitation of energy-dispersive X-ray spectroscopy has hindered the direct detection of organic carbon occurrence within smectite interlayers, impeding the exploration of interaction mechanism between organic carbon and clay minerals at the nanostructure level. Recently, Liu et al. utilized a unique resin-embedding sectioning method and energy loss spectroscopy to detect the distribution of silicon and carbon in clay minerals of source rocks and red earth [24,25]. Their study demonstrated that silicon primarily coexists within clay mineral interlayers where silicon is less abundant, revealing the structural characteristics of organic carbon-clay mineral

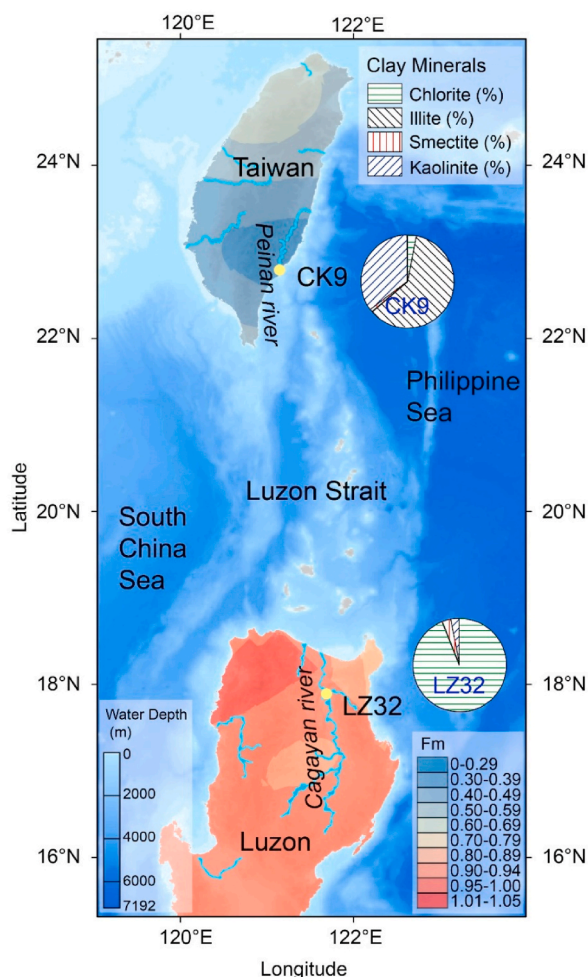


**Fig. 1.** Distribution of radiocarbon activity of total organic carbon (reported as “fraction modern”, Fm) in fluvial surficial sediments on Taiwan and Luzon. The Fm map is generated by interpolation of widely distributed fluvial sediments, thus only representing statistical features of surficial sediments, but not for rock, soil, and vegetation on land. Locations of samples CK9 from Taiwan and LZ32 from Luzon are indicated. Pie charts show clay mineral assemblages of the two samples. Fm data from Lin et al. [28,29]; clay mineral data from Liu et al. [26,27].

interlayer complex.

In this study, X-ray photoelectron spectroscopy (XPS), Fourier transform infrared spectroscopy (FTIR), and transmission electron microscope (TEM) coupled with energy dispersive spectroscopy (EDS) and electron energy loss spectroscopy (EELS) were used to investigate the effects of clay minerals on the composition and spatial distribution of organic matter in fluvial sediments. The objective of this study is to provide a nanoscale perspective on the transport and preservation processes of terrestrial organic carbon.

## 2. Samples and methods

### 2.1. Samples and pretreatment

Two sediment samples collected from the Peinan River in Taiwan and the Cagayan River in Luzon were used for microscopic analysis (Fig. 1). Previous studies on the clay mineralogy of these two samples indicated that the sample collected from Taiwan (CK9) were primarily composed of illite and chlorite, while the sample collected from Luzon (LZ32) were predominantly composed of smectite. And comparing to CK9, LZ32 has higher mineral surface area (SA) and lower median grain size (Table 1) [26,27]. Furthermore, previous geochemical investigations revealed differences in the organic carbon composition between the two samples. The organic carbon in CK9, which has lower total organic carbon (TOC) and total nitrogen (TN), primarily originated from ancient rocks, i.e., petrogenic carbon, whereas the organic carbon in LZ32 with higher TOC is mainly derived from soils, i.e., pedogenic carbon (Table 1) [28,29]. These differences in clay minerals and organic carbon compositions between CK9 and LZ32 signify the inherent association between clay minerals and organic carbon.

Prior to the laboratory work, samples were soaked in 1 M HCl for 16 h at room temperature (25 °C) to remove carbonates and then rinsed five times with Milli-Q water to remove any trace of HCl.

### 2.2. XPS and FTIR analyses

XPS is a surface-sensitive technique that provides quantitative information on all elements (except for H and He) present on the surface, with a penetration depth of approximately 10 nm [30]. In this study, the 10 nm penetration depth of XPS enables the detection of organic carbon information in the interlayer of clay minerals. XPS analysis was conducted using a Thermo Fisher K-Alpha instrument equipped with an Al K $\alpha$  source (excitation energy = 1468.6 eV at 400  $\mu$ m X-ray spot) in the CAS Key Laboratory of Mineralogy and Metallogeny in Guangzhou Institute of Geochemistry. The XPS analysis chamber was evacuated to an ultrahigh vacuum (pressure  $\leq 5 \times 10^{-8}$  mbar) prior to analysis. For wide scanning, the pass energy was set to 100 eV, while for narrow scanning, it was set to 30 eV. Peak fitting of the XPS C1s signal was achieved using the Gauss-Lorentz method to separate the spectrum into five peaks, based on carbon speciation, with a  $\pm 0.1$  eV tolerance and a full width at half maximum of  $1.6 \pm 0.2$  eV (Table 2). It is worth noting that the  $sp^2$  carbon peak shape is asymmetric and has a tail in the high binding energy region. However, in view of the small content of  $sp^2$  carbon in the sample in this study, the influence on the content of other components in the high-energy region is limited.

FTIR absorbance spectra were obtained using a Bruker Vertex 70 FT-IR spectrometer (Manheim, Germany) in the CAS Key Laboratory of Mineralogy and Metallogeny in Guangzhou Institute of Geochemistry. Pure spectroscopic-grade KBr (Aladdin, China) was measured and used as a reference. Each specimen used for FTIR measurement was prepared by blending and grinding 0.9 mg of sample powder with 80 mg of KBr, followed by pressing the mixture into a wafer. The spectra were collected over 64 scans in the range of 4000–400  $cm^{-1}$  with a resolution of 4  $cm^{-1}$ . Band positions were assigned based on previous investigations and by considering the predominant clay mineralogy of the samples [31–34].

### 2.3. TEM coupled with EDS and EELS analyses

This study employed two sample preparation methods, droplet method and ultra-thin section method, for TEM sample preparation. Firstly, 100 mg of  $<2 \mu$ m clay fraction was dispersed in 10 ml of deionized water. The sample was then subjected to 5 min of ultrasonic dispersion to ensure thorough dispersion. Next, 20  $\mu$ L of the dispersion was quickly dropped onto a microgrid copper mesh and allowed to air dry. The prepared samples were stored in a drying oven until testing.

The ultrathin section method, described extensively in a previous paper [24], was used to facilitate the observation of clay mineral (00l) planes under a microscope. In this method, resin was injected into a mold with dimensions of  $2.0 \times 1.0 \times 1.0$  cm until it occupied approximately half of the volume. The mold was then placed in an oven, and the resin was cured at 70 °C for 15 h. Subsequently, a well-dispersed suspension with 1% clay content was dropped onto the resin and allowed to air dry, promoting the oriented

**Table 1**

Organic geochemical and clay mineralogical compositions of typical fluvial samples CK9 in Taiwan and LZ32 in Luzon.

Sample Name	Longitude (°E)	Latitude (°N)	SA (m <sup>2</sup> g <sup>-1</sup> )	Median grain size ( $\mu$ m)	TOC (%)	TN (%)	$\delta^{13}C$ (‰)	F <sub>m</sub>	Chlorite (%)	Illite (%)	Smectite (%)	Kaolinite (%)
CK9	121.14	22.79	4.59	24.9	0.42	0.07	-22.1	0.14	35	60	3	1
LZ32	121.69	17.89	49.80	6.4	0.89	0.10	-24.9	1.06	3	0	94	3

Note: Organic geochemistry data from Lin et al. [28,29]; clay mineral data from Liu et al. [26,27]; F<sub>m</sub>, fraction modern of radiocarbon activity.

**Table 2**  
Assignment of XPS peak positions in the C1s-K2p region [35].

Binding Energy (eV)	Attribution
aliphatic hydrocarbon	
284.0	C $sp^2$
285.0	C $sp^3$
Oxidized organic carbon	
286.5	C–O
287.7	C=O
289.2	O–C=O

arrangement of clay minerals on the resin surface. The resin was further injected until the mold was filled, followed by another 15-h curing period at 70 °C. The solidified samples were cut along the smallest plane and vertically to the largest plane using a diamond knife (Microstar Standard) and the Leica EM UC7 Ultramicrotome. Ultrathin sections with thicknesses of 50–80 nm were placed on copper grids without carbon film coating for TEM characterization, with the (001) planes of clay particles preferentially oriented parallel to the incident direction of electron beams.

High-angle annular dark-field scanning TEM images and EDS results were collected using a FEI Talos F200S field-emission transmission electron microscope operating at an accelerating voltage of 200 kV. High-resolution TEM analysis was performed using an FEI TITAN G2 field-emission transmission electron microscope with an accelerating voltage of 200 kV. The EELS study was conducted using the Gatan Quantum EELS accessory with a voltage of 200 kV. Line scans were recorded by the electron beams with steps of 0.2 nm.

### 3. Results

#### 3.1. Organic carbon compositions of fluvial sediments

XPS results show that organic carbons in the samples are in five types, including olefin, saturated hydrocarbon, alcohol (or ether), ketone (or aldehyde), and acid (or ester) (Fig. 2). Their binding energies are 284.0, 285.0, 286.5, 287.7, and 289.2 eV, respectively. The first two types (olefin and saturated hydrocarbon) are organic carbons combined with hydrogen, belonging to aliphatic hydrocarbons, while the other three types (alcohol, ketone, and acid) are organic carbons combined with oxygen (Table 3). The peaks between 292 and 298 eV are due to the peak of potassium (the peak of K2p 1/2 and K2p 3/2) and the  $\pi-\pi^*$  shake-up satellite peaks of aromatic hydrocarbons (Fig. 2) and will not be discussed here [36].

The organic carbon compositions of Taiwan and Luzon samples are very different (Table 3). The aliphatic hydrocarbon compounds show a higher proportion of  $sp^2$  C in LZ32 than in CK9, indicating that the Luzon sample contains higher alkenes. Additionally, CK9 has a significantly lower fraction of oxidized organic carbon (fCO<sub>x</sub>) value compared to LZ32 (Fig. 2a). The signals of C–O and C=O functional groups are more prominent in LZ32 (Fig. 2b), indicating the presence of more alcohol (or ether) and ketone (or aldehyde) compounds (Table 3). However, there is no significant difference between the two samples regarding more strongly oxidized acid (or

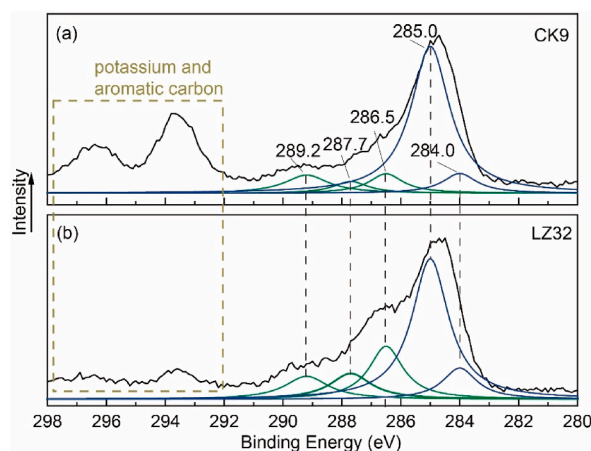


**Fig. 2.** XPS spectra and peak fitting results in C1s-K2p region for CK9 from Taiwan (a) and LZ32 from Luzon (b). The spectra (black line) are categorized into seven peaks according to Table 2, representing saturated hydrocarbons (blue line), carbon bonded to oxygen (green line), and peaks associated with potassium and aromatic carbon (tan dashed rectangle). To facilitate a direct comparison between the two samples, vertical dotted lines are utilized to connect peaks with identical positions. (For interpretation of the references to color in this figure legend, the reader is referred to the Web version of this article.)

**Table 3**  
Relative contents of organic carbon compositions calculated from the XPS analysis.

Species	CK9	LZ32
Aliphatic hydrocarbon		
C $sp^2$	0.08	0.11
C $sp^3$	0.69	0.51
Oxidized organic carbon		
C–O	0.08	0.18
C=O	0.05	0.11
O–C=O	0.10	0.10
fCO <sub>x</sub>	0.23	0.38

ester) compounds.

### 3.2. Binding of clay minerals and organic carbon in fluvial sediments

The results of FTIR show that the combination of organic carbon and clay minerals makes the infrared absorption bands of the two samples slightly offset, but the deviation direction of different types of infrared absorption bands is different. The infrared absorption bands of organic carbon in LZ32 showed slight redshifts compared with CK9. In CK9, the bands corresponding to the stretching vibrations of methyl C–H, carboxyl C=O, and the bending vibration of C–H appear at 2926, 1638, and 1425  $cm^{-1}$ , respectively (Fig. 3a). In LZ32, the corresponding bands positions are 2925, 1637, and 1423  $cm^{-1}$  (Fig. 3b). Compared with LZ32, the infrared absorption bands in CK9 related to the octahedral sheet of clay minerals are redshifted, but the bands related to the tetrahedral sheet are not shifted. The bands at 1028 and 526  $cm^{-1}$  in CK9 represent the stretching vibration of Si–O and the deformation vibration of Al–O–Si, respectively (Fig. 3a). In LZ32, these bands occur at positions 1032 and 527  $cm^{-1}$ , respectively (Fig. 3b). On the other hand, the absorption bands at 3441, 788, and 471  $cm^{-1}$  represent the hydroxyl group in the clay mineral structure, stretching vibration of Si–O–Si and deformation vibration of Si–O, respectively, and no differences were observed in these bands between the two samples (Fig. 3).

### 3.3. Spatial combination between clay minerals and organic carbon

In CK9, organic carbon is closely bound to illite, and organic carbon is evenly distributed on illite. The lower part of Fig. 4a, characterized by lighter-colored plate-like minerals rich in O (Fig. 4d), Mg (Fig. 4e), Al (Fig. 4f), Si (Fig. 4g), and K (Fig. 4h), is identified as illite. Additionally, well-defined crystalline iron oxides can be observed in the left part of field of view (Fig. 4i). After excluding the influence of the carbon film on the backside of the copper grid, no localized aggregation or enrichment of C (Fig. 4b) and N (Fig. 4c) on the surface of clay minerals is observed. This suggests that the organic carbon is evenly distributed on the illite particles.

Similar characteristics were also observed in the distribution of organic carbon and clay minerals in LZ32. The primary minerals in Fig. 5a are identified as smectite, containing elements such as O (Fig. 5d), Mg (Fig. 5e), Al (Fig. 5f), Si (Fig. 5g), and Ca (Fig. 5i). The elongated particles rich in K (Fig. 5h), appearing in the lower left of the field of view, are determined to be illite. Additionally, circular

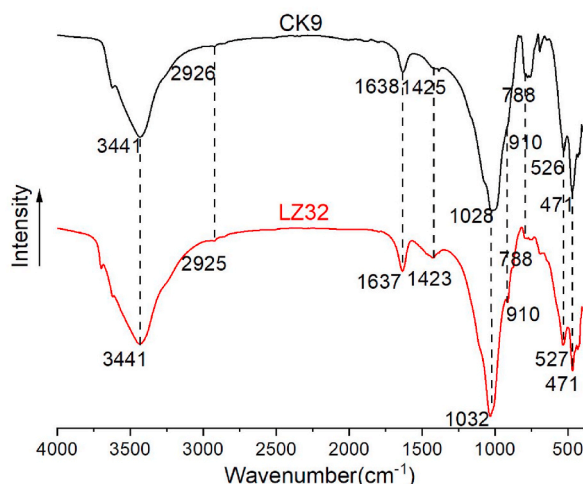


**Fig. 3.** FTIR spectra of CK9 from Taiwan (a) and LZ32 from Luzon (b). The absorption characteristic bands of clay minerals and organic carbon are marked with positions. To establish connections between the two samples, vertical dotted lines are used to link the corresponding characteristic bands.

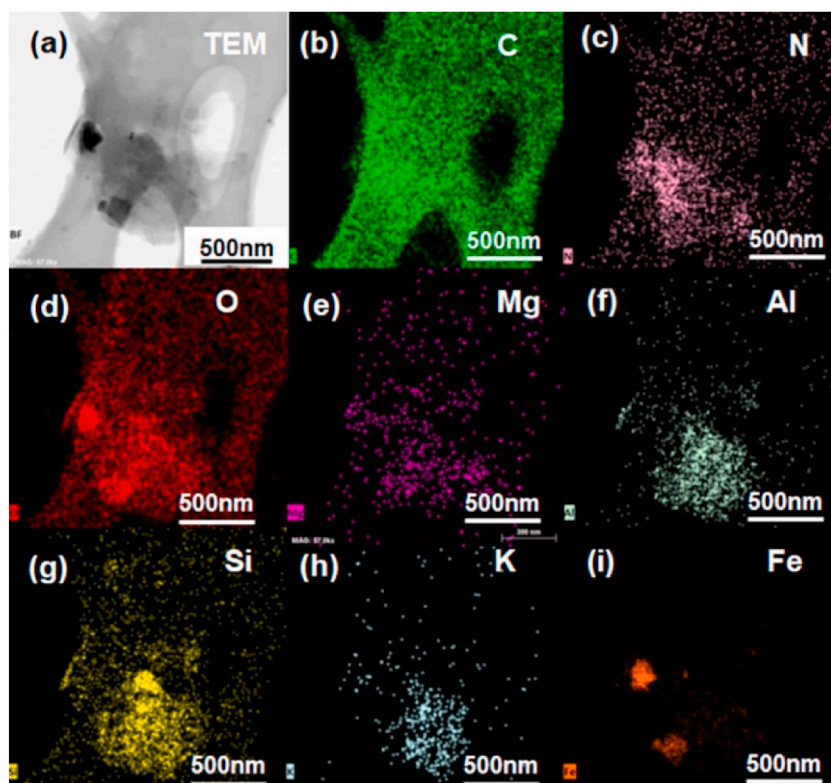


Fig. 4. TEM image (a) and EDS mapping results of C (b), N (c), O (d), Mg (e), Al (f), Si (g), K (h), and Fe (i) of mineral-organic carbon complex in CK9 from Taiwan.

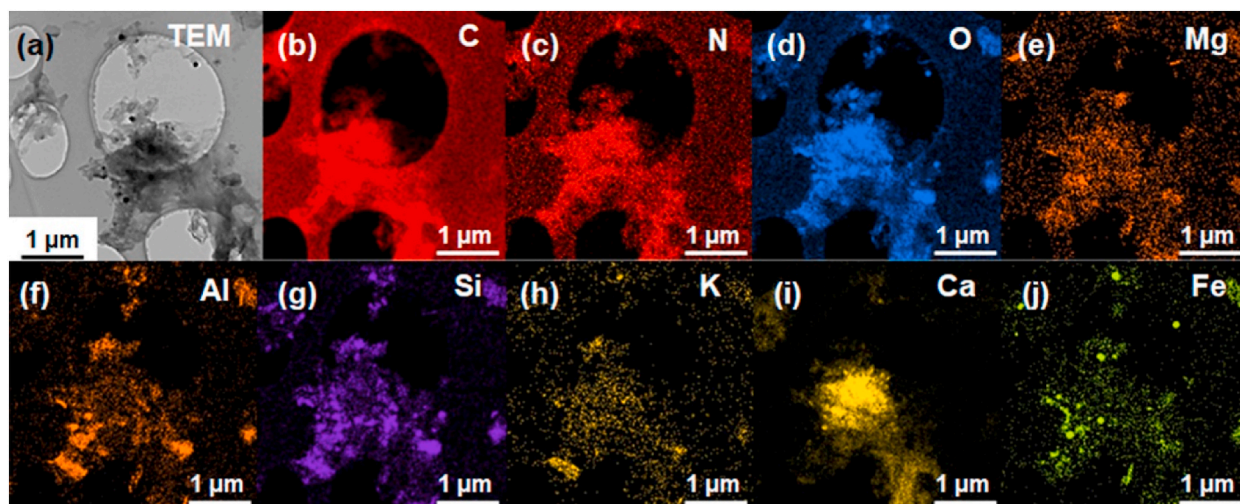


Fig. 5. TEM image (a) and EDS mapping results of C (b), N (c), O (d), Mg (e), Al (f), Si (g), K (h), Ca (i), and Fe (j) of minerals-organic carbon complexes in LZ32 from Luzon.

iron oxide particles with diameters ranging from approximately 20–30  $\mu\text{m}$  are present in the sample (Fig. 5j). Similarly, the spatial distribution of C (Fig. 5b) and N (Fig. 5c) does not exhibit localized aggregation or enrichment, indicating that organic carbon is uniformly distributed on the clay minerals. Additionally, the different clay minerals, smectite and illite, do not show differences in the binding of organic carbon.

### 3.4. Organic carbon in clay mineral nanolayer structure

The high-angle annular dark-field scanning TEM image of illite in CK9 clearly shows the tightly arranged illite layers, separated by a wider layer of smectite (Fig. 6a). The basal spacing of illite is measured to be approximately 1.0 nm, while the wider interlayer region has a basal spacing of 1.4 nm, as observed in the inverse fast Fourier transformed image (Fig. 6b). In the case of LZ32, the layer structure of smectite is more distinct, with regularly arranged basal spacing of 1.4 nm, as shown in Fig. 6c and d.

The EELS results indicate that the Si content is high in the smectite layers and low in the interlayer regions in smectite of LZ32. On the other hand, carbon shows a significant negative correlation with the Si content, with high values observed in the interlayer regions. In CK9, the Si signal in the illite also exhibits the characteristic of higher intensity in the bright regions and relatively lower intensity in the dark regions, indicating that EELS detected the layering structure of the clay mineral. However, the distribution of carbon does not show typical layering-related features but appears as random fluctuations.

## 4. Discussions

### 4.1. Influence of clay minerals on spatial distribution of organic matters

The macroscopic binding relationship between organic carbon and clay minerals is roughly the same in Taiwan and Luzon samples, but the slight shifts of FTIR bands indicates the difference of organic carbon binding between smectite and illite. EDS results show that the binding of different clay minerals to organic carbon is tight and uniform. The elements representing organic carbon, such as C and N, have a good spatial coupling relationship with the elements representing clay minerals, such as Si and Al. However, FTIR results show differences in organic carbon binding between different clay minerals. The slight shifts of organic carbon characteristic bands towards lower wavenumbers in LZ32 is likely due to hindered infrared vibrations caused by the close association between organic carbon and the mineral surfaces [37]. Therefore, the degree of association between organic carbon and clay minerals is tighter in the Luzon sample compared to the Taiwan sample. Besides, the redshift of bands reflects information about octahedral sheets in clay minerals of CK9, indicating that there may be more organic carbon attached to the edge defects of octahedral sheets in the Taiwan sample [38,39].

High-resolution TEM coupled with EELS results reveal the effect of different structure of clay minerals on the nanoscale spatial distribution of organic carbon. The clay minerals in the Taiwan sample are mainly illite, whose interlayer space is small and non-expandable. There is no obvious correlation between Si and C, indicating that the distribution of C in illite is not affected by the layer structure. The clay minerals in the Luzon sample are mainly smectite, whose interlayer space can expand and contract according to the change of environment. The EELS analysis shows that the Si and C in the layer structure are negatively correlated to each other, indicating that organic carbon mainly exists in the interlayer space of smectite [24]. Combining the information obtained by FTIR and EELS, it is obviously that there is a large difference in the occurrence of organic carbon in the two sediments. In the smectite rich Luzon fluvial sediments, organic carbon mainly occurs in the interlayer space of clay minerals. While in the illite rich river sediments in Taiwan, organic carbon mainly occurs at the surface and edge defects of clay minerals.

### 4.2. Selective combination of organic carbon functional groups with clay minerals

The source and age of organic carbon have a significant impact on the types of organic carbon. Previous studies on carbon isotopes have revealed that the organic carbon in the CK9 sample primarily originates from ancient rock organic carbon [28], while LZ32 predominantly contains pedogenic organic carbon [29]. The organic carbon in the sample of Taiwan has undergone burial and diagenesis for thousands of years, and the initial C–O and C=O functional groups may have been decomposed or transformed during burial diagenesis. This explains why the oxidized organic carbon content in the Taiwan sample is smaller than that in the Luzon sample.

However, the inorganic minerals also have a potential impact on the composition of organic carbon. The close contact between organic carbon and illite edge in Taiwan sample may explain the high acid content in the organic carbon composition [40]. The oxygen in organic carbon can form bonds with positively charged edges of clay minerals [37,41]. This close metal-bridging effect can provide spatial protection for organic carbon, allowing it to preserve a higher acid content. However, the organic carbon in Luzon samples tends to be preserved in the interlayer of clay minerals. Although the oxidized organic carbon content is high, the negatively charged acid organic carbon is difficult to enter the interlayer region of smectite [42], resulting in a relatively small proportion of organic carbon components. In conclusion, the type of organic carbon in fluvial sediments is mainly controlled by the source and age of organic carbon. In addition, the selective combination of inorganic minerals is also an important factor affecting the composition of organic matters.

### 4.3. Effect of clay mineral nanostructure on organic carbon preservation

It is noteworthy that organic carbon tends to present in the interlayer space of smectite, while rarely in that of illite. This observation emphasizes the significance of the internal surface area of smectite in its adsorption capacity for organic carbon [43]. Measuring the internal surface area of smectite using common gas adsorption-desorption methods is challenging due to its interlayer space being only 0.3–0.5 nm, which is smaller than the kinetic diameter of gas molecules like N<sub>2</sub> and CO<sub>2</sub> [44]. As a result, the internal surface area can only be determined through adsorption tests using organic molecules such as ethylene glycol monoethyl ether [45]. Previous

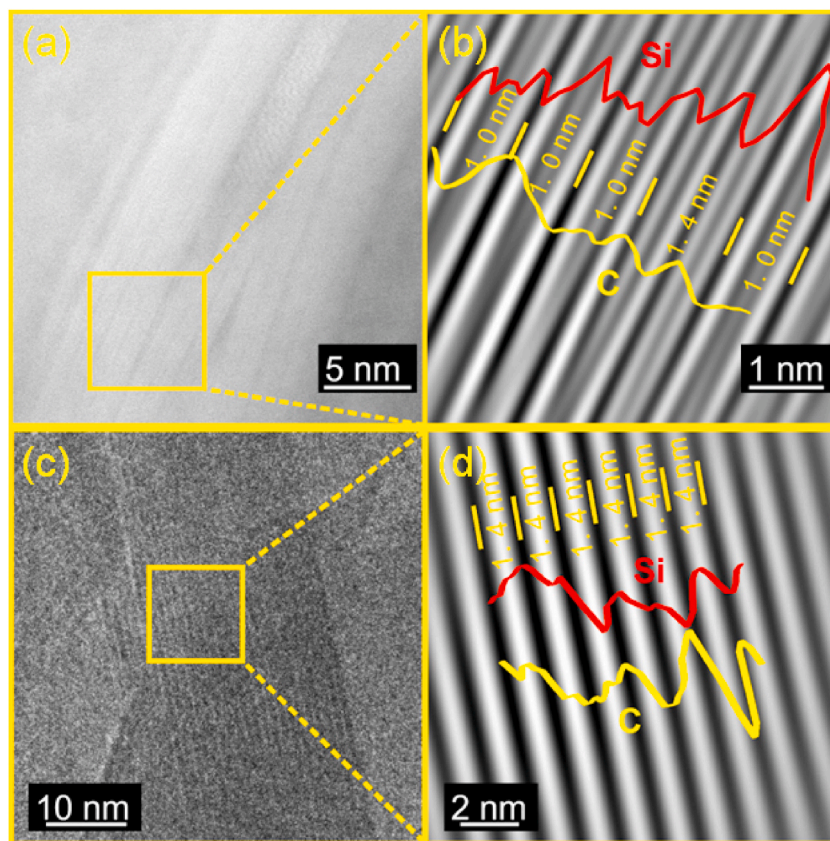


**Fig. 6.** High-angle annular dark-field scanning TEM and high-resolution TEM images of clay minerals in CK9 from Taiwan and LZ32 from Luzon. (a) High-angle annular dark-field scanning TEM image of illite (CK9). (b) Inverse fast Fourier transformed image of the zoom position in (a). (c) High-resolution TEM image of smectite (LZ32). (d) Inverse fast Fourier transformed image of the zoom position in (d). The short yellow lines represent the basal spacing of clay minerals. The EELS line scan results of C (yellow curve) and Si (red curve) show no clear correlation in illite but show negative correlation in smectite. (For interpretation of the references to color in this figure legend, the reader is referred to the Web version of this article.)

studies have indicated that the internal surface area of smectite is typically 7–8 times larger than its external surface area [46]. Therefore, the adsorption and sequestration of organic carbon in the expandable interlayer of smectite should not be ignored.

On the other hand, not all expandable clay minerals uniformly adsorb organic carbon on their inner surfaces. In this study, the illite rich Taiwan fluvial samples also have smectite layers with wide spacing (1.4 nm), but there is no organic carbon in the space between these layers (Fig. 6b). Therefore, it is not accurate to determine the location of organic carbon in clay minerals simply based on the type and structure of clay minerals. When studying the adsorption behavior of organic carbon on clay minerals, it is necessary to use transmission electron microscopy to detect the presence or absence of organic carbon in the interlayer space of clay minerals in different samples.

However, the effect of the interlayer nanocomposite structure of smectite and its interaction with organic carbon on the preservation of organic carbon requires further investigation. On the one hand, compared to the outer surface, the interlayer space provides a narrower environment that enhances the thermal stability of organic carbon and offers protection against decomposition by biological enzymes [47–49]. On the other hand, this nanocomposite structure also offers a larger reaction interface. In aqueous environments, the interlayer space of smectite may undergo further expansion [50,51], potentially leading to a loss or more rapid exchange of nanoscale interlayer organic carbon. As a result, conducting more refined experiments becomes essential to verify the stability of interlayer organic carbon under different environmental conditions.

## 5. Conclusions

In this study, we conducted XPS, FTIR, and TEM analyses on typical fluvial samples from Taiwan and Luzon to investigate the nanoscale association between clay minerals and organic carbon. The results revealed a close association between organic carbon and clay minerals in sediments. Specifically, in Taiwan samples, organic carbon was predominantly bound to illite edges, whereas in Luzon samples, it was found in the interlayer space of smectite. The content of oxidized organic carbon in Taiwan samples was found to be smaller than that in Luzon samples. This difference is primarily influenced by the type and age of organic carbon, as well as the selective combination of inorganic clay minerals. These findings provide valuable insights into the influence of different clay mineral

nano-layer structures on the occurrence of organic carbon. As a result, they offer a theoretical foundation for understanding the role of clay minerals in the transport and preservation of organic carbon.

## Data availability

Data generated in this study are reported as figures and tables of this manuscript.

## CRediT authorship contribution statement

**Hongzhe Song:** Writing – review & editing, Writing – original draft, Methodology, Data curation, Conceptualization. **Zhifei Liu:** Writing – review & editing, Supervision, Investigation, Funding acquisition, Conceptualization. **Baozhi Lin:** Writing – review & editing, Methodology, Data curation. **Yulong Zhao:** Writing – review & editing, Investigation. **Fernando P. Siringan:** Writing – review & editing, Resources. **Chen-Feng You:** Writing – review & editing, Resources.

## Declaration of competing interest

The authors declare that they have no known competing financial interests or personal relationships that could have appeared to influence the work reported in this paper.

## Acknowledgements

We sincerely thank Shunai Che and Lu Han for their help in TEM experiments and data processing. We thank Editor Dr. Andrew Hursthouse for handling the manuscript and two anonymous reviewers for their constructive comments on the early version of this paper. This work was supported by the National Natural Science Foundation of China (42130407, 42188102, 42306066) and the Interdisciplinary Project of Tongji University (ZD-22-202102).

## References

- [1] R. Mikutta, G.E. Schaumann, D. Gildemeister, S. Bonneville, M.G. Kramer, J. Chorover, O.A. Chadwick, G. Guggenberger, Biogeochemistry of mineral–organic associations across a long-term mineralogical soil gradient (0.3–4100 kyr), Hawaiian Islands, *Geochem. Cosmochim. Acta* 73 (2009) 2034–2060.
- [2] R.T. Conant, M.G. Ryan, G.I. Ågren, H.E. Birge, E.A. Davidson, P.E. Eliasson, S.E. Evans, S.D. Frey, C.P. Giardina, F.M. Hopkins, Temperature and soil organic matter decomposition rates—synthesis of current knowledge and a way forward, *Global Change Biol.* 17 (2011) 3392–3404.
- [3] M. Schrumpf, K. Kaiser, G. Guggenberger, T. Persson, I. Kögel-Knabner, E.-D. Schulze, Storage and stability of organic carbon in soils as related to depth, occlusion within aggregates, and attachment to minerals, *Biogeosciences* 10 (2013) 1675–1691.
- [4] A.M. Ahmat, M. Boussafir, C. Le Milbeau, R. Guégan, T. De Oliveira, L. Le Forestier, Organic matter and clay interaction in a meromictic lake: implications for source rock OM preservation (Lac Pavin, Puy-de-Dôme, France), *Org. Geochem.* 109 (2017) 47–57.
- [5] S. Arndt, B.B. Jørgensen, D.E. LaRowe, J. Middelburg, R. Pancost, P. Regnier, Quantifying the degradation of organic matter in marine sediments: a review and synthesis, *Earth Sci. Rev.* 123 (2013) 53–86.
- [6] X. Sun, D. Fan, L. Hu, Z. Yang, Z. Guo, Oxidation of petrogenic organic carbon in a large river-dominated estuary, *Geochem. Cosmochim. Acta* 338 (2022) 136–153.
- [7] B. Sarkar, M. Singh, S. Mandal, G.J. Churchman, N.S. Bolan, Clay Minerals—Organic Matter Interactions in Relation to Carbon Stabilization in Soils. *The Future of Soil Carbon*, 2018. Elsevier 71–86.
- [8] J. Chang, X. Fan, Z. Jiang, X. Wang, L. Chen, J. Li, L. Zhu, C. Wan, Z. Chen, Differential impact of clay minerals and organic matter on pore structure and its fractal characteristics of marine and continental shales in China, *Appl. Clay Sci.* 216 (2022) 106334.
- [9] S.T. Droge, K.-U. Goss, Development and evaluation of a new sorption model for organic cations in soil: contributions from organic matter and clay minerals, *Environ. Sci. Technol.* 47 (2013) 14233–14241.
- [10] Q. Fan, M. Tanaka, K. Tanaka, A. Sakaguchi, Y. Takahashi, An EXAFS study on the effects of natural organic matter and the expandability of clay minerals on cesium adsorption and mobility, *Geochem. Cosmochim. Acta* 135 (2014) 49–65.
- [11] U. Kuila, D.K. McCarty, A. Derkowski, T.B. Fischer, T. Topór, M. Prasad, Nano-scale texture and porosity of organic matter and clay minerals in organic-rich mudrocks, *Fuel* 135 (2014) 359–373.
- [12] S. Boyd, M. Mortland, Enzyme interactions with clay and clay-organic matter complexes, in: J. Bollag, G. Stotzky (Eds.), *Soil Biochemistry*, Marcel Dekker, Inc., USA, 1990, pp. 1–128.
- [13] H.-R. Schulten, P. Leinweber, New insights into organic-mineral particles: composition, properties and models of molecular structure, *Biol. Fertil. Soils* 30 (2000) 399–432.
- [14] Q. Li, L. Wang, Y. Fu, D. Lin, M. Hou, X. Li, D. Hu, Z. Wang, Transformation of soil organic matter subjected to environmental disturbance and preservation of organic matter bound to soil minerals: a review, *J. Soils Sediments* 23 (2023) 1485–1500.
- [15] C. Feller, E. Schouller, F. Thomas, J. Rouiller, A.J. Herbillon, N<sub>2</sub>-BET specific surface areas of some low activity clay soils and their relationships with secondary constituents and organic matter contents, *Soil Sci.* 153 (1992) 293–299.
- [16] L.M. Mayer, B. Xing, Organic matter–surface area relationships in acid soils, *Soil Sci. Soc. Am. J.* 65 (2001) 250–258.
- [17] S.A. Schweizer, C.W. Mueller, C. Höschen, P. Ivanov, I. Kögel-Knabner, The role of clay content and mineral surface area for soil organic carbon storage in an arable toposequence, *Biogeochemistry* 156 (2021) 401–420.
- [18] A.U. Dogan, M. Dogan, M. Onal, Y. Sarikaya, A. Aburub, D.E. Wurster, Baseline studies of the clay minerals society source clays: specific surface area by the Brunauer Emmett Teller (BET) method, *Clay Clay Miner.* 54 (2006) 62–66.
- [19] F. Macht, K. Eusterhues, G.J. Pronk, K.U. Totsche, Specific surface area of clay minerals: comparison between atomic force microscopy measurements and bulk-gas (N<sub>2</sub>) and-liquid (EGME) adsorption methods, *Appl. Clay Sci.* 53 (2011) 20–26.
- [20] M.J. Kennedy, S.C. Löhner, S.A. Fraser, E.T. Baruch, Direct evidence for organic carbon preservation as clay-organic nanocomposites in a Devonian black shale; from deposition to diagenesis, *Earth Planet Sci. Lett.* 388 (2014) 59–70.
- [21] M.L. Droser, J.G. Gehling, M.E. Dzaugis, M.J. Kennedy, D. Rice, M.F. Allen, A new Ediacaran fossil with a novel sediment displacive life habit, *J. Paleontol.* 88 (2014) 145–151.
- [22] C. Su, Y. Liu, Y. Yang, T. Gao, T. Qi, Y. Wang, Evolution of aromatic structure and nanopores in shale kerogen by using in-situ HRTEM and in-situ FT-IR experiment, *Fuel* 359 (2024) 130479.

- [23] H. Zhu, C. Huang, Y. Ju, H. Bu, X. Li, M. Yang, Q. Chu, H. Feng, P. Qiao, Y. Qi, P. Ma, M. Zheng, Y. Lu, Multi-scale multi-dimensional characterization of clay-hosted pore networks of shale using FIBSEM, TEM, and X-ray micro-tomography: implications for methane storage and migration, *Appl. Clay Sci.* 213 (2023) 106239.
- [24] D. Liu, Q. Tian, P. Yuan, P. Du, J. Zhou, Y. Li, H. Bu, J. Zhou, Facile sample preparation method allowing TEM characterization of the stacking structures and interlayer spaces of clay minerals, *Appl. Clay Sci.* 171 (2019) 1–5.
- [25] D. Liu, M. Li, R. Yu, H. Li, Y. Shen, Q. Tian, H. Bu, C. Huang, W. Tan, Interlayer organic matter within hydroxy-interlayered clay minerals enhances soil organic carbon stability under long-term organic fertilization, *Appl. Clay Sci.* 239 (2023) 106963.
- [26] Z. Liu, S. Tuo, C. Colin, J.T. Liu, C.-Y. Huang, K. Selvaraj, C.-T.A. Chen, Y. Zhao, F.P. Siringan, S. Boulay, Detrital fine-grained sediment contribution from Taiwan to the northern South China Sea and its relation to regional ocean circulation, *Mar. Geol.* 255 (2008) 149–155.
- [27] Z. Liu, C. Colin, X. Li, Y. Zhao, S. Tuo, Z. Chen, F.P. Siringan, J.T. Liu, C.-Y. Huang, C.-F. You, Clay mineral distribution in surface sediments of the northeastern South China Sea and surrounding fluvial drainage basins: source and transport, *Mar. Geol.* 277 (2010) 48–60.
- [28] B. Lin, Z. Liu, T.I. Eglinton, S. Kandasamy, T.M. Blattmann, N. Haghypour, K.-F. Huang, C.-F. You, Island-wide variation in provenance of riverine sedimentary organic carbon: a case study from Taiwan, *Earth Planet Sci. Lett.* 539 (2020) 116238.
- [29] B. Lin, Z. Liu, T.I. Eglinton, T.M. Blattmann, S. Kandasamy, N. Haghypour, F.P. Siringan, Organic matter compositions and loadings in river sediments from humid tropical volcanic Luzon Island of the Philippines, *J. Geophys. Res.-Bio.* 126 (2021) e2020JG006192.
- [30] M.J. Bock, L.M. Mayer, Mesodensity organo–clay associations in a near-shore sediment, *Mar. Geol.* 163 (2000) 65–75.
- [31] H.W. Van der Marel, H. Beutelspacher, *Atlas of Infrared Spectroscopy of Clay Minerals and Their Admixtures*, Elsevier, Amsterdam, 1976.
- [32] J. Madejova, P. Komadel, Baseline studies of the clay minerals society source clays: infrared methods, *Clay Clay Miner.* 49 (2001) 410–432.
- [33] J. Peuravuori, A. Monteiro, L. Eglite, K. Pihlaja, Comparative study for separation of aquatic humic-type organic constituents by DAX-8, PVP and DEAE sorbing solids and tangential ultrafiltration: elemental composition, size-exclusion chromatography, UV–vis and FT-IR, *Talanta* 65 (2005) 408–422.
- [34] G.O. Akintola, F. Amponsah-Dacosta, S. Rupprecht, N. Palaniyandy, S.E. Mhlongo, W.M. Gitari, J.N. Edokpayi, Methanogenesis potentials: insights from mineralogical diagenesis, SEM and FTIR features of the permian mikambeni shale of the Tuli basin, Limpopo province of South Africa, *Minerals* 11 (2021) 651.
- [35] J.A. Donadelli, A. Canneva, G. Erra, A. Calvo, XPS direct analysis on shale rocks: correlation with kerogen type and maturity, *Fuel* 257 (2019) 116004.
- [36] D.J. Morgan, Comments on the XPS analysis of carbon materials. *C* 7 (3) (2021) 51.
- [37] Q. Wu, Z. Li, H. Hong, Adsorption of the quinolone antibiotic nalidixic acid onto montmorillonite and kaolinite, *Appl. Clay Sci.* 74 (2013) 66–73.
- [38] H. Slosiariková, J. Bujdák, V. Hlavatý, IR spectra of octadecylammonium-montmorillonite in the range of the Si-O vibrations, *J. Incl. Phenom. Mol. Recognit. Chem.* 13 (1992) 267–272.
- [39] J. Du, J. Cai, Z. Chen, T. Lei, S. Zhang, Z. Xie, A contrastive study of effects of different organic matter on the smectite illitization in hydrothermal experiments, *Appl. Clay Sci.* 168 (2019) 249–259.
- [40] W.H. Yu, N. Li, D.S. Tong, C.H. Zhou, C.X.C. Lin, C.Y. Xu, Adsorption of proteins and nucleic acids on clay minerals and their interactions: a review, *Appl. Clay Sci.* 80 (2013) 443–452.
- [41] J.P. Ferris, Mineral catalysis and prebiotic synthesis: montmorillonite-catalyzed formation of RNA, *Elements* 1 (3) (2005) 145–149.
- [42] N. Loganathan, B.O. Ferguson, B. Arey, H.E. Argersinger, G.M. Bowers, A mechanistic exploration of natural organic matter aggregation and surface complexation in smectite mesopores, *J. Phys. Chem. A* 124 (47) (2020) 9832–9843.
- [43] P. Barré, O. Fernandez-Ugalde, I. Virto, B. Velde, C. Chenu, Impact of phyllosilicate mineralogy on organic carbon stabilization in soils: incomplete knowledge and exciting prospects, *Geoderma* 235 (2014) 382–395.
- [44] B. Theng, G. Ristori, C. Santi, H. Percival, An improved method for determining the specific surface areas of topsoils with varied organic matter content, texture and clay mineral composition, *Eur. J. Soil Sci.* 50 (1999) 309–316.
- [45] H. Bu, D. Liu, P. Yuan, X. Zhou, H. Liu, H. Song, B. Zhang, Ethylene glycol monoethyl ether adsorption by interlayer montmorillonite-organic matter complexes: dependence on the organic matter content and its alkyl chain length, *Appl. Clay Sci.* 180 (2019) 105190.
- [46] J. Srodon, D.K. McCarty, Surface area and layer charge of smectite from CEC and EGME/H<sub>2</sub>O-retention measurements, *Clay Clay Miner.* 56 (2008) 155–174.
- [47] H. Liu, P. Yuan, Z. Qin, D. Liu, D. Tan, J. Zhu, H. He, Thermal degradation of organic matter in the interlayer clay–organic complex: a TG-FTIR study on a montmorillonite/12-aminolauric acid system, *Appl. Clay Sci.* 80 (2013) 398–406.
- [48] P. Yuan, H. Liu, D. Liu, D. Tan, W. Yan, H. He, Role of the interlayer space of montmorillonite in hydrocarbon generation: an experimental study based on high temperature–pressure pyrolysis, *Appl. Clay Sci.* 75 (2013) 82–91.
- [49] C. Merino, R. Godoy, F. Matus, Soil enzymes and biological activity at different levels of organic matter stability, *J. Soil Sci. Plant Nutr.* 16 (1) (2016) 14–30.
- [50] W.P. Gates, Crystalline swelling of organo-modified clays in ethanol–water solutions, *Appl. Clay Sci.* 27 (1–2) (2004) 1–12.
- [51] T. Okada, J. Oguchi, K.I. Yamamoto, T. Shiono, M. Fujita, T. Iiyama, Organoclay in water cause expansion that facilitates caffeine adsorption, *Langmuir* 31 (1) (2015) 180–187.